Final Draft
Manuscript available at: https://doi.org/10.1061/(ASCE)BE.1943-5592.0000539
Full citation: Russell, BR, Thrall, AP, Padula, JA, and Fowler, JE (2014) "Reconceptualization and Optimization of a Rapidly Deployable Floating Causeway." Journal of Bridge Engineering, 19(4), 04013013

Re-Conceptualization and Optimization of a Rapidly Deployable Floating Causeway

Brittani R. Russell, S.M.ASCE[1]; Ashley P. Thrall, A.M.ASCE [2]; Joseph A. Padula [3]; Jimmy E. Fowler [4];

ABSTRACT

There is an increasing demand for rapidly deployable causeways that can provide access from ship to shore for military and disaster relief operations. Existing systems have major limitations including only being transportable and emplaceable by large strategic sealift vessels, having high weight and packaged volumes, and requiring intensive on-site assembly. In response to the demand for a lightweight, air-liftable, quickly emplacable causeway, the Engineer Research and Development Center has developed a prototype comprised of aluminum modules joined by compliant connections and supported by pneumatic floats. As research and development progressed and experience was gained, eliminating the heavy and complex compliant connections was identified as a potential improvement. To eliminate these compliant connections, the authors have re-conceptualized this design so that a desired superstructure flexibility (that takes advantage of buoyancy while meeting deflection limits) is achieved. The superstructure has been designed for a target stiffness to permit a desired curvature under a design moment. This paper will (1) review existing causeways, (2) present this re-conceptualization, and (3) discuss the optimization implemented to achieve this new design.

CE Database subject headings: Bridges; Floating structures; Military engineering; Composite material; Optimization

[1]Graduate Student, Department of Civil and Environmental Engineering and Earth Sciences, University of Notre Dame, Notre Dame, IN 46556. E-mail: brussel2@nd.edu

[2]John Cardinal O'Hara, C.S.C. Assistant Professor, Department of Civil and Environmental Engineering and Earth Sciences, University of Notre Dame, Notre Dame, IN 46556. (corresponding author) E-mail: athrall@nd.edu

[3]Research Civil Engineer, Geotechnical and Structures Laboratory, US Army Engineer Research and Development Center, Vicksburg, MS 39180 E-mail: joseph.a.padula@usace.army.mil

[4]Associate Technical Director, Coastal Hydraulics Laboratory, US Army Engineer Research and Development Center, Vicksburg, MS 39180 E-mail: jimmy.e.fowler@usace.army.mil

INTRODUCTION

Causeways, meaning bridging systems capable of transporting troops and supplies from ship to shore, are a critical military asset to reach austere or damaged sites. The Department of Defense has identified a strategic interest in reaching these sites by shallow-draft vessels with rapidly deployable causeways for offloading operations or disaster relief (Deming, 2009). Existing causeways can provide access to these damaged and small ports, but have the major limitation of only being transportable and emplaceable by deep-draft vessels with high-load capacity cranes. Furthermore, existing systems have a high weight and packaged volume, require intensive in-water assembly with substantial support equipment, and cannot be transported by air (Fowler et al., 2006; Deming, 2009). Toward this end, a prototype was developed by the Engineer Research and Development Center (ERDC), known as the Lightweight Modular Causeway System (LMCS, Figure 1), with technical support from Alion Science and Technology, Demaree Inflatable Boats, Oceaneering International Incorporated, and Quantum Engineer Design Incorporated (Deming, 2009). This system is a modular, floating causeway comprised of aluminum modules joined by compliant connections and supported by pneumatic floats.

The existing prototype demonstrates a reduction in packaged volume and self-weight by at least 50% compared to other existing systems. A 36.6 m LMCS causeway can be shipped in the footprint of three International Standards Organization (ISO) freight containers (Deming, 2009), but the system is still somewhat heavier than the developers would like. The compliant connections between modules are fairly complex and make up a large component of the system self-weight. Toward this end, the authors have re-conceptualized this system such that the connections can be simplified and the required rotational compliance is achieved in the module instead. This is accomplished by designing a cross section with a target stiffness to permit a specific rotation under a given load. A box girder profile is assumed. The design of this section is performed using multi-objective structural optimization to minimize the self-weight of the section while reaching the target stiffness. This procedure is performed first for a glass fiber reinforced polymer (GFRP) material to explore opportunities for the use of advanced composites for lightweight design. An analogous procedure is also performed to design optimized cross sections in two grades of high strength steel. All three resulting designs are compared against the existing prototype.

This paper will first briefly review the history of causeway systems developed by the US military, focusing on its newest design. Then it will discuss the desired re-conceptualization of the superstructure assembly. Next, the multi-objective optimization process will be discussed, including a review of relevant work in the field, a detailed problem formulation, and a description of the algorithm employed - Simulated Annealing (SA). Finally, the optimized designs will be presented and compared against the existing prototype.

A BRIEF REVIEW OF CAUSEWAY SYSTEMS AND THE EXISTING PROTOTYPE

To better understand the context for this re-conceptualization, it is critical to review (1) the history of deployable and rapidly erectable causeway systems starting after World War II and leading up to the current effort and (2) the existing prototype, including its advantages over prior systems and potential areas for improvement.

History of Causeway Systems

The history of deployable and rapidly erectable causeway systems begins with a temporary harbor that was used by the Allied forces during World War II - the Mulberry Harbour. Although the system proved invaluable until it was destroyed by a large storm, the harbor system was not replicated (Potts, 2009). Later systems were designed to be more transportable, less challenging logistically, and are briefly presented below.

Two of the earliest fielded causeway systems were the Navy Lighterage System (NLS) in the 1960's and the Modular Causeway System (MCS) in the 1980s. Both consist of steel modular sections. The modules of the NLS are 6.40 m wide by 27.43 m long. Since they are so large, the modules require special lifting equipment to be put in place and they are not ISO compatible (able to be handled by ISO material handling equipment and transported by ISO compatible vehicles and trailers) (Garala, 2004; Anon., 2012). The MCS, which was adopted by the U.S. Army, was designed to be ISO compatible and can be configured in several different ways: the Floating Causeway, the Roll-On/Roll-Off discharge facility, the Causeway Ferry, and the Warping Tug. All can be interchanged and connected both side-to-side and end-to-end (Buonopane, 2002; Department of Defense Office of the Inspector General, 2004). Both of these systems are only capable of operating through Sea State 2 (SS2, refer to Fort Eustis Weather (2012) for definitions of sea states) conditions, and improvements were made upon them for future causeway solutions (Garala, 2004; Fort Eustis Weather, 2012).

The Navy Elevated Causeway System (ELCAS) and the Navy Modular Elevated Causeway System (ELCAS (M)) were designed in 1975 and 1985 respectively. To this day, the ELCAS is one of the most efficient deployable causeway systems to transport supplies over the surf-line. It is made from modular sections which are elevated on piles 6.10 m above water (Groff, 1992). Construction of this system begins at the beach where the piles are driven into the ground and the modules are connected between them (Lin, 1999). Initially the modules float on the water, and one by one they are lifted up and welded together (Skaalen and Rausch, 1977). The modular version was designed to facilitate quicker deployment (Groff, 1992). The 6.40 m wide causeway and turntable at the end allow for two-way traffic over the system. The intent was that this system would be operable in SS3 conditions, but it can only be operated through SS2 (Deitchman, 1993).

In 1991 the Joint Modular Lighter System (JMLS) was designed to address the shortcomings in the NLS and the MCS. Specifically, there existed interest to operate during SS3 conditions, but the system was only safe to operate through SS2 (Garala, 2004). Similar to the MCS, the 12.19 m long by 2.44 m wide by 2.44 m high JMLS modules can be connected both side-to-side and end-to-end and can be made as powered or non-powered configurations. Unfortunately, several deficiencies were found with this system. Cracking in the welds between modules was seen with SS2 and above, the side connector system was problematic, and the many obstructions on the deck proved hazardous to personnel (Garala, 2004). The JMLS was replaced by the Improved Navy Lighterage System (INLS) that was designed in the 1990's. It is comprised of the same overall size and configuration as the JMLS, but incorporated improved side connectors that overcame the JMLS deficiencies. Operation is possible through SS3 conditions, the system is able to sustain only minimal damage under SS4, and it can structurally survive a SS5 event (Garala, 2004).

Despite these successes enjoyed by the MCS and INLS systems, both require strategic sealift assets to transport and deploy. This is a major drawback for rapid response operations by high speed shallow-draft vessels that could significantly shorten main supply routes by use of austere points of entry (such as damaged or small ports) that are much closer to the final destination. This is the main factor that led to the development of the LMCS. The reader is referred to Russell and Thrall (2013) for a review of portable and rapidly deployable bridges that provides additional detail on each of these systems with supporting images.

Existing LMCS Prototype

In order to address the shortcomings of existing causeway solutions for emergency response using shallow-draft vessels, a rapidly deployable floating causeway known as the LMCS was developed (Figure 1). The existing prototype is comprised of 3.05 m long by 6.10 m wide modular units having an aluminum superstructure and pneumatic floats. The modules can be connected end-to-end to form a floating bridge or a floating causeway. High strength, but lightweight fabric is used for the floats to avoid puncture and abrasion. To take greater advantage of the buoyancy of the floats, the system must offer some flexibility. In the existing design, this flexibility is achieved by compliant connections - with a specific rotational compliance to provide this flexibility while meeting deflection limits - between the modules (Deming, 2009).

Based on the demand indicated by the Department of Defense and the shortcomings of existing solutions, design priorities for the LMCS included (1) the ability to be transported aboard and deployed from shallow-draft vessels for use in austere environments (such as mudflats and wetlands) and damaged ports or harbors (with shallow water or soft soil conditions), (2) the ability to be transported by land, air, and in an ISO compatible configuration, (3) easy assembly without substantial support equipment, and (4) low self-weight and packaged volume (Fowler et al., 2006; Deming, 2009). With these priorities in mind, the LMCS was designed to have minimal draft when unladen and be capable of increasing shoreline accessibility in shallow instances by partially deflating floats on the leading edge as it is pushed or winched into position. For easy transportation, the LMCS was designed to be shipped in an ISO compatible configuration and transportable by land, sea, or air. A key advantage in this respect, is that the system, unlike its predecessors, can be transported by the Joint High Speed Vessel (Fowler et al., 2006). Incorporation of these priorities will allow deployable causeways to access significantly shallower ports than was possible with previous systems. A 36.6 m causeway can be deployed by 7 people in 3 hours. The main actions required to deploy the structure are to inflate the floats by one of several methods and to join the modules together and activate the pinning mechanisms. The system can be retrieved in a comparable amount of time. The causeway is capable of supporting multiple M1A2 Main Battle Tanks when sufficient distance is allowed between them. The LMCS currently is 36.6 m comprised of 12 modules that each provide 3.05 m of traveled way. In addition to being used in a Vessel to Shore Bridging mode, it has also been used successfully in a wet gap crossing application. During April 2010, the LMCS was used in a post earthquake response exercise in connection with Exercise Arctic Edge 2010 in Alaska. This drill was completed by only 20 soldiers using organic equipment to offload and emplace 21.3 m of LMCS to provide an expedient floating bridge on the Eagle River. In order to secure the bridge against the current after deployment, it was anchored to land with several mooring lines. Other simulations were performed to demonstrate the utility of the system at an austere landing site and delivery via helicopter (Ferguson, 2010).

RE-CONCEPTUALIZATION

Though this system shows great promise and has performed well in recent field experiments and assessments, areas for further improvement include eliminating the compliant connections. These connections are complicated in design and are heavy, making up approximately half of the self-weight of each module. The goal of this research, therefore, was to re-conceptualize the existing design to eliminate these compliant connections. More specifically, the rotational compliance of the existing hinges was selected to permit sufficient rotation to take advantage of the buoyancy of the floats. Figure 2 represents three different configurations for a floating causeway, where the curved line indicates the water level. If the system is stiff, meaning that full moment connections exist between modules, then the structure cannot take full advantage of buoyancy between wave peaks (Figure 2A). The existing prototype, instead, employed compliant connections between modules to better utilize this effect (Figure 2B, with a closeup of this connection shown in Figure 3A) (Resio et al., 2012). Since the connections are both heavy and complex, we aimed to eliminate the connections by transferring the rotational compliance to the deck itself (Figure 2C). This can be achieved by reducing the stiffness of the deck to a target value to achieve a specific rotation under a given load. Here, the target was for .08 radians of rotation over a 3.05 m long module under 1,140 kNm load (representing the design bending moment when the causeway is supporting one M1A2 tank and the ramp load) (Resio et al., 2012). Modules can then be connected using lighter, simpler fixed connections as proposed in Figure 3B. For transportation, modules could be disconnected.

In addition to eliminating the compliant connections, we also changed the cross-section to a box girder and investigated the use of advanced composite material and steel. Advanced composite materials were considered since they are lightweight and corrosion resistant, which is especially critical in salt-water environments that causeways experience. GFRP has been widely used in structural engineering projects and, since it is significantly less expensive than other advanced composites such as carbon fiber-reinforced polymers (CFRP), it was chosen for this research. Two versions of high strength steel were also considered as viable options for the re-conceptualization.

STRUCTURAL OPTIMIZATION OF RE-CONCEPTUALIZED CAUSEWAY

The design of deployable structures is a particularly challenging problem since self-weight and packaged volume are at a premium to permit transportability, and ultimately feasibility. Structural optimization is a useful tool to fully explore the design space. For the re-conceptualized system, we have implemented multi-objective structural optimization to minimize the self-weight and the stiffness, subject to the constraints of a minimum target value for the stiffness, structural criteria based on the Pre-Standard for Load & Resistance Factor Design (LRFD) of Pultruded Fiber Reinforced Polymer (FRP) Structures manual by the American Society of Civil Engineers (LRFD manual, hereafter) (ASCE, 2010), and geometric requirements. This section will first review relevant research in this area and then present the problem formulation and algorithm employed.

Structural optimization has been used in the past to more efficiently design floating decks.

One example of this is a study to determine the optimal layout of gill cells in very large floating structures (VLFS) to minimize the differential deflection of the system due to non-uniform loading (Wang et al., 2007; Pham and Wang, 2010). The introduction of specific cells which allow water to flow freely in and out can reduce this differential deflection by up to 66% (Pham and Wang, 2010). Studies have been made to determine the optimal number and location of these cells for various shaped VLFS. Circular structures produce a differentiable and continuous optimization function. Therefore, sequential quadratic programming, a classical optimization algorithm based on Newton's method, was used (Wang et al., 2007). When optimizing the arrangement of the gill cells in an arbitrarily shaped section with any loading configuration, the genetic algorithm was utilized (Pham and Wang, 2010).

Optimization strategies have also been used in the design of permanent bridge decking systems. Many of these have been in response to the deterioration of existing bridges. The most widely used optimization algorithm for this type of analysis is the Genetic Algorithm (GA) because of its capabilities to escape local minima and to handle discrete and non-differentiable optimization functions. GA and Shuffled Frog Leaping were utilized to determine which bridge decks in a region should be repaired first (Elbehairy et al., 2006). Multi-objective GA has also been used to determine bridge deck rehabilitation so that the total rehabilitation cost and the weighted average deterioration degree were minimized. With the many solutions given by multi-objective optimization, a bridge owner would then be able to select the best combination for his or her particular case (Liu et al., 1997). As mentioned previously, fiberglass reinforced polymers (FRP) are also becoming popular in bridge deck rehabilitation projects. However, a substantial up-front cost is typically required for these components. While the examples given above aim to reduce the life-time cost of the bridge system, the optimization examples given below are geared at reducing this initial cost so that FRP is a more appealing option to bridge owners. To achieve this goal, the volume of the decking system is minimized. This has been done on its own (Dey et al., 2013), and also in conjunction with optimization of the FRP material composition (Park et al., 2005; He and Aref, 2003). GA was used for all three of these studies. Finally, in order to account for uncertainties such as those that exist in the material properties, structural dimensions, and applied loads, another study was performed to simultaneously consider a finite element model, the optimization algorithm, and a reliability analysis procedure (Thompson et al., 2006).

Problem Formulation

For the proposed re-conceptualization, the authors sought a low-weight design with a target stiffness. To achieve this goal, multi-objective structural optimization for minimum self-weight and minimum moment of inertia (related to stiffness by young's modulus) was implemented, with a constraint that the moment of inertia not be below the target value. Additional constraints include that the design meet the structural requirements of the LRFD manual and geometric criteria related to function and packaging. The design variables relate to the box girder cross-section, including the depth of the entire cross-section (H), the thickness of the top and bottom flanges (t_{ft} and t_{fb}, respectively), the width of the bottom flange (w_{fb}), and the thickness of the exterior webs (t_{we}) (Figure 4). These variables are permitted to range from 9.5 to 6,096 mm in 3.2 mm increments. The minimum thickness and discrete increment size is based on the manufacturing capabilities for FRP members. The number (n) and thickness of the interior webs (t_{wi}) are determined within the algorithm to ensure compliance with all code requirements. Additionally shown in Figure 4 are the width of the top flange (w_{ft}) which is a fixed value of 6,096 mm based on functionality requirements, the height of the webs (h_w), and the horizontal width of the exterior flange (b_{we}). These last two variables are geometrically related to the design variables in the following way:

$$h_w = H - t_{ft} - t_{fb} \tag{1}$$

$$b_{we} = \frac{t_{we}}{\sin\left(\arctan \frac{h_w}{0.5(w_{ft} - w_{fb})}\right)} \tag{2}$$

These are used to simplify equations presented here.

The formal definition of this optimization problem is as follows:

$$
\begin{aligned}
\underset{H,t_{ft},t_{fb},w_{fb},t_{we}}{\text{minimize}} \quad & W(s) = p(t_{ft}w_{ft} + t_{fb}w_{fb} + 2b_{we}h_w + n_{wi}t_{wi}h_w) \\
& I_x(s) = \sum_{i=1}^{nel}(I_{xi} + A_i d_i^2) \\
\text{such that} \quad & c_i \leq 0; i = 1, \ldots, u
\end{aligned}
\tag{3}
$$

where W refers to the self-weight of the superstructure, which is the summation of the area of each of the of elements times the density (p) of the GFRP material. The moment of inertia objective function (I_x) is simply found by the parallel axis theorem, where d is the distance from an individual component's centroid to that of the overall superstructure assembly's. Finally, the cross section produced by the algorithm must conform to the u number of constraints, c, related to the minimum value for the moment of inertia (c_1), structural constraints of the LRFD manual (c_2-c_6), and geometric constraints (c_7-c_8) related to design criteria for use and packaging. Prior three-dimensional finite element analyses of the system, performed by the ERDC, provide the design moment, shear, and torsion acting on the system due to load combinations prescribed by Trilateral Design code which include the effects of dead, vehicle, wave, ramp, and damaged pontoon loads (Resio et al., 2012; Federal Republic of Germany, United Kingdom & United States of America, 1996). Table 1 provides these values. A load factor of 1.33, which was the largest load factor provided in the Trilateral Design code, was then conservatively applied to each to enable design by LRFD (Federal Republic of Germany, United Kingdom & United States of America, 1996). These values would need to be adjusted for the final detailed design, but they provide sufficient detail for this stage of the design process. The LRFD manual was used for minimum values for material properties. If these values were not available, then the appropriate values were taken from the design manual Fiberglass Grating and Structural Products by Delta Composites (Delta Composites L.L.C., 2004).

The first constraint, c_1, ensures that the superstructure moment of inertia does not allow greater flexibility of the system than desired by setting a lower limit on this value, as follows:

$$c_1 = M_s \frac{\rho}{E_L} - I_x \leq 0 \tag{4}$$

where ρ is the desired radius of curvature, M_s is the bending moment under service load (Table 1), and E_L is the longitudinal modulus of elasticity. In using this moment-curvature relationship, we are assuming that plane sections remain plane and linear elastic material behavior. Given a desired rotation of .08 radians over a 3.05 m long module under a uniform bending moment, the target (minimum) moment of inertia is 0.003503 m^4.

Structural constraints were defined by the criteria in the LRFD manual, related to shear (strength of members due to material rupture in shear, to web shear buckling, and to web lateral stability), flexure (strength of members due to material rupture and due to local instability), torsion (torsional capacity when strength governs), and concentrated load requirements (strength of members due to tensile rupture in the webs, to web crippling, to web compression buckling, and to flange flexural failure). Lateral torsional buckling and torsional effects related to warping and bending have not been included since these effects are generally negligible for closed box sections. The following paragraphs will detail each of these structural constraints. For all the calculations it was assumed that all GFRP components have the same material properties and that no delamination or separation occurs between them.

The LRFD design for members in shear is based on the governing behavior between material rupture in shear and web shear buckling. The shear capacity (V_n) must exceed the demand (V_u):

$$c_2 = V_u - \lambda \phi V_n \leq 0 \tag{5}$$

where λ is a time effect factor and ϕ is the resistance factor for shear. For this calculation as well as for all others presented in this document, λ = 0.8 (ASCE, 2010). The shear demand on the system is the design value identified in Table 1 multiplied by the 1.33 load factor. For material rupture in shear, ϕ = 0.65 and V_n is calculated as $V_n = F_{LT} A_s$, where F_{LT} is the characteristic in plane shear strength, and A_s is the shear area ($A_s = H b_{we}$). This shear area was conservatively assumed to be the area of a single web. In reality the shear would be transferred through the section by several, or all, of the webs. However, since the exact distribution of the contribution from each web could only be known by a detailed finite element analysis, the most conservative assumption was made that any individual web must be able to carry the entire demand. For the final design the web widths could be reduced after a detailed analysis was performed to determine the actual demand on each web. For web shear buckling, ϕ = 0.80 and V_n is found by $V_n = F_{cr}A_s$, where f_{cr} is the critical shear buckling stress, a function of the design variables t$_{we}$ and H. The reader is referred to the LRFD manual for this equation (ASCE, 2010). Note that these constraints consider the adequacy of the external webs only. The design of the internal webs are discussed at the end of this section of the paper.

The next two constraints check the adequacy of the section against the flexural demands. The constraint c$_3$ ensures that the material will not rupture in bending. The bending capacity (M_n) must exceed the demand (M_u) as follows:

$$c_3 = M_u - \lambda\phi M_n \leq 0 \tag{6}$$

where the resistance factor, ϕ, is 0.65. The nominal flexural strength, is calculated as $M_n = \frac{F_L I_x}{y}$, where F_L is the longitudinal flexural strength and y is the distance from the neutral axis of the cross section to the extreme fiber of the member. Here M_u is the factored moment, defined as 1.33 times the design moment in Table 1. The second flexural constraint checks that the external webs are thick enough to prevent local instability. The constraint is defined as:

$$c_4 = t_{we\,r} - t_{we} \leq 0 \tag{7}$$

where t$_{we\ r}$ represents a required web thickness that can be found by rearranging the equations from section 5.2.3 of the LRFD manual as follows:

$$t_{we\,r} = \sqrt{\frac{6H^2}{11.1\pi^2(1.25\sqrt{E_{L,w}E_{T,w}} + E_{T,w}\nu_{LT} + 2G_{LT})}\frac{M_u y}{\lambda\phi I_x}} \tag{8}$$

where ϕ = 0.80, $E_{L,w}$ and $E_{T,w}$ are respectively the longitudinal and transverse modulus of elasticity in the web, ν_{LT} is the longitudinal poisson's ratio, and G_{LT} is the in plane shear modulus. The flanges and internal webs were also checked against local instabilities and are discussed in further detail later.

The fifth constraint, c_5, relates to the torsional capacity of the member, and is defined as

$$c_5 = T_u - \lambda\phi T_n \leq 0 \tag{9}$$

where T_u is the required torsional demand (1.33 times the design value in Table 1), ϕ is 0.70, and T_n is the nominal torsional capacity. The torsional capacity for a closed section can be calculated as $T_n = 2tF_{LT}A_o$, where t is conservatively taken to be the minimum thickness of any of the exterior elements and A_o is the area enclosed by the centerline of the exterior elements (Beer et al., 2006).

For concentrated loads, the load demand (R_u) must exceed the capacity (R_n) as follows:

$$c_6 = R_u - \lambda\phi R_n \leq 0 \tag{10}$$

The demand arises from concentrated wheel loads from M1A2 Abrams Main Battle Tank and from the ramp which connects the ship to the causeway. The ramp load was considered to be a special loading scenario which the entire causeway system need not be able to withstand. It was assumed that special detailing would be considered in the module which would withstand the ramp load. Therefore, the concentrated load was taken to be the weight of the M1A2 tank divided by the number of wheels (R_u=68kN, including the load factor). Three limit states (tensile rupture, web crippling, and compressive buckling) are included in this constraint. For all three of these checks, both the internal and the external webs were analyzed, and the smallest ϕR_n value from the three checks governed. For tensile rupture in the webs, $R_n = l_{ten}F_{T,w}t_w$, where l_{ten} is the depth of the webs, and $F_{T,w}$ is the transverse flexural strength of the webs. It was again conservatively assumed that a single web was required to carry the entire load. Therefore, t_w was taken as the width of the thinnest web (either t_{we} or t_{wi}). For this limit state, ϕ is 0.65. For web crippling, ϕ = 0.70 and $R_n = 0.7h_w t_w F_{sh,int}(1 + \frac{2k+6t_{plate}+b_{plate}}{d_w})$, where $F_{sh,int}$ is the interlaminar shear strength and k is defined as the distance from the top of the member to the bottom of the fillet. Since no fillet exists in the cross-section this was taken as the thickness of the top flange, t_{ft}. t_{plate} and b_{plate} refer to the thickness and length of the bearing plate. Since no bearing plate exists, this again was taken as the thickness of the top flange and the maximum allowable value of 102 mm, respectively. d_w is the depth of the web, which is h_w in this case. For web compression buckling, ϕ = 0.80 and $R_n = f_{cr}A_{eff}$, where A_{eff} is the effective area ($A_{eff} = l_{eff}t_w$, where l_{eff} is the lesser of the web depth (d_w) or the distance between vertical stiffeners) and f_{cr} is

$$f_{cr} = \frac{\pi^2 t_w^2}{6l_{eff}^2}(\sqrt{E_{L,w}E_{T,w}} + E_{T,w}\nu_{LT} + 2G_{LT}) \tag{11}$$

One more concentrated load check appears in the LRFD manual. This last equation is associated with the stability of the flange and is discussed later.

The remaining constraints are geometric, relating to functional needs, packaging requirements, and physical constraints. The angle between the top and bottom flange must be greater than 45%, which can be expressed formally as:

$$c_7 = w_{ft} - w_{fb} - 2H \leq 0 \tag{12}$$

For packaging, the depth of the cross section must be shallow enough to allow four modules to fit in the footprint of one ISO container (which corresponds to a maximum depth of 400mm):

$$c_8 = H - 400\text{mm} \leq 0 \tag{13}$$

The final two geometric constraints ensure that the algorithm does not specify a cross section that is physically impossible. Specifically, the thickness of the top and bottom flanges cannot be greater than the depth of the entire member:

$$c_9 = t_{ft} + t_{fb} - H \leq 0 \tag{14}$$

and the thickness of the external webs cannot be greater than the width of the cross section:

$$c_{10} = 2t_{we} - w_{ft} \leq 0 \tag{15}$$

The number and thickness of the internal webs have not been set as design variables, but instead have been calculated to meet various limit states. The required number of internal webs is based on meeting stability criteria for the flanges. This includes the strength of the compression flange member due to local instability induced by flexure on the entire cross section and against flange flexural failure caused by a concentrated force. The equation to determine the required number of internal webs (n_{wi}) based on the former of these is too complex to include here. It is based on Sections 5.2.3 and 5.2.3.4, part a of the LRFD manual, "Compression flange local buckling for square and rectangular box members". Since both the top and the bottom flange of the cross section can go into compression it was necessary to perform this analysis on each of them. The calculation for n_{wi} based on concentrated load demands is:

$$n_{wi} = \frac{3W_{ft}R_u}{\lambda\phi F_{T,f}t_{ft}^2} - 1 \tag{16}$$

where $F_{T,f}$ is the transverse flexural strength in flange, and ϕ = 0.65. n_{wi} is taken as the governing value between these two calculations. It was assumed that the internal webs were spaced evenly across the section and that the concentrated force acted in the most critical location, that is midway between two webs. The web thickness was determined by the governing calculation between the material rupture in shear, web shear buckling, and the flexural local instability. These first two checks are derived from the same equations as described in c_2; the equations were simply rearranged to solve for t_{wi} (which replaces b_{we} and t_{we} in the c_2 equations). Similarly, the required thickness of the internal webs based on the flexural instability check is identical to that described in c_4. As was the case with the external web calculations, it was conservatively assumed that each individual web would be required to carry the entire shear demand.

As noted earlier, we performed an analogous procedure for two types of high strength steel - A709 HPS 70 steel (483MPa yield strength) and A709 HPS 100 steel (689 MPa yield strength). The design variables and objective functions remain the same, but the structural constraints (c_2-c_6) are replaced by the constraints from the American Association of State Highway and Transportation Officials (AASHTO) LRFD Bridge Design Specifications (AASHTO, 2012) for the design of steel box girders. The target moment of inertia (c_1) was also changed to achieve the same desired stiffness with a different modulus of elasticity (0.000217 m^4).

Simulated Annealing

The authors chose to approach their problem using Multi-Objective Simulated Annealing (MOSA). Heuristic algorithms, such as Simulated Annealing (SA), are intuitive, relatively quick, and are capable of handling the continuous and discrete constraints in current structural design codes. For the specific applications of bridge engineering, simulated annealing has been used to design reinforced concrete box road structures (Perea et al., 2008), bridge piers (Martinez-Martin et al., 2012), prestressed concrete and tensegrity footbridges (Martí and González-Vidosa, 2010; Ali et al., 2010), for shape and sizing optimization of linkage-based movable bridges (Thrall et al., 2012), and to identify moving axle loads to aid in design (in conjunction with Genetic Algorithms) (Qu et al., 2011). Note that this is a non-exhaustive review of the implementation of SA for bridge design, but serves to highlight potential applications of this algorithm in this field. The authors have already demonstrated the effectiveness of SA for the design of deployable structures comprised of linkages (Thrall et al., 2013; Thrall, 2011).

SA is an iterative improvement algorithm that is based on an analogy to crystal formation. In the physical process of annealing, as the melted mass is slowly cooled, the energy of the system gradually decreases. During this process there is a probability (P) that a higher energy configuration can occur, which ultimately leads to a lower energy configuration. This probability is given by the formula, $P = e^{\frac{-\Delta E}{T}}$ where ΔE refers to the difference in the energy configurations and T is the temperature of the mass. As the temperature is decreased there is a lower probability that a higher energy state will occur (Kirkpatrick et al., 1983). This process can be extended to structural optimization. This was first proposed by Kirkpatrick et al. (1983), where the probability relates to the probability of accepting higher value functions and energy relates to the existing function, therefore enabling the algorithm to escape local minima. T is a variable that con be controlled by the user. A high temperature is used initially to widely explore the solution space and is slowly decreased as the algorithm converges (Kirkpatrick et al., 1983).

For single objective SA (e.g minimum weight optimization), the algorithm begins by selecting an initial solution by randomly generating a feasible set of design variables from a database of discrete values specified by the user. This set becomes the initial best solution. One or more of the variables are then randomly perturbed to generate a new solution. If this solution conforms to all constraints and produces a lower weight solution, it becomes the new current solution. If not, there is a certain probability, as discussed above, that it can still be accepted as the current solution upon which the algorithm continues to iterate. The algorithm explores the solution space for a user defined number of iterations in a cooling cycle. The temperature is decreased at the end of each cooling cycle, thereby decreasing the probability that a higher weight solution will be accepted. In other words, the algorithm's ability to escape a local minimum decreases. Convergence is defined as a certain number of cooling cycles in which there has been no improvement in the solution. The final result is the lowest weight solution (Kirkpatrick et al., 1983).

This process of optimizing a single design variable can be extended to multi-objective optimization. Rather than combining objective functions using a weighted average, the objective functions remained separated to produce a pareto-optimal set of solutions. Solutions are pareto-optimal if they are not overshadowed by other solutions in either objective function. At convergence a pareto-optimal set gives the designer an array of possible solutions spanning between extremes that one would find through single objective optimization. Based on the design priorities, a designer can select a final solution (Suppapitnarm et al., 2000).

Optimized Designs

By nature, heuristic algorithms are not guaranteed to converge on the same solution each time they are employed. The user defines several parameters, including v (the maximum number of variables to be varied at once), pm (the amount of perturbation permitted along the database of allowable values), r (the factor by which the temperature is reduced), m (the length of a cooling cycle), and n (the number of cooling cycles for convergence of the algorithm). The quality and robustness of the algorithm are dependent on the selection of these parameters. To determine a robust selection of these parameters for multi-objective optimization, single objective optimization was performed for each objective function using 16 different combinations of the parameters, v, pm, r, m, and n. Twenty numerical simulations were performed for each combination. Table 2 provides the combinations considered as well as the average result (μ), standard deviation (σ), and coefficient of variation for the GFRP design (c_v). The most robust combination (where robustness is defined as having both a low average and a low standard deviation) for both objective functions is SA 4 ($v = 1$, $pm = 10$, $r = 0.8$, $m = 10,000$, and $n = 2$, highlighted in bold in Table 2).

With this selection of parameters, MOSA was performed for the GFRP design to find a pareto-optimal set of results from which a designer can select a final design (Figure 5, empty circles). The diamond and square show the best results from single objective optimization of the weight and moment of inertia, respectively, representing the extremes between which the pareto-optimal set spans. The dotted horizontal line shows the target moment of inertia value. The authors chose the cross section shown as a black filled circle as the best combination of moment of inertia and weight. This solution had a moment of inertia close to the target value (0.003504 m^4), with an acceptable weight (1,208 kg/m, including the weight of the floats). The corresponding cross section is shown in Figure 6A. An analogous procedure was performed for the two grades of steel and the resulting optimized cross sections are shown in Figure 6B,C.

The optimized results are summarized and compared against the existing LMCS system in Table 3. For all three optimized designs, the desired system stiffness was achieved (or closely approached). Therefore, the compliant connections can be eliminated as desired and replaced by the simplified option shown in Figure 3B. In addition to simplifying the connection detail, one of the highest priorities was reducing the total system weight. Table 3 provides the weight of the modules alone (W, without hinges or floats), the weight of the modules with connections (no floats), and the total system weight which includes the floats. Note that it was assumed that the simplified connections proposed for the re-conceptualized system would have a negligible impact on the weight of the entire system. Unfortunately, the GFRP design was not able to reduce the system weight below that of the existing prototype. This is largely due to local constraints on the top flange. Both steel designs showed lower weights than the GFRP option, with the 689 MPa grade option having a lower system weight than the existing system. Furthermore, the total superstructure depth (H) is reduced, thereby enabling additional modules to fit within the footprint of an ISO container. This offers the potential to reduce the time and cost for transportation to the site. Overall, these results are very promising.

CONCLUSIONS AND FUTURE WORK

The authors have presented a re-conceptualized, rapidly deployable causeway with the use of multi-objective structural optimization for GFRP and two grades of high strength steel. The resulting designs (Figure 6, Table 3) are highly promising, with each meeting (or approaching) the desired target stiffness to replace the heavy and complex compliant connections (Figure 3A) with a proposed simplified connection (Figure 3B). It is expected that this proposed connection will be simpler, lighter, and easier to deploy and maintain than the compliant connections of the original prototype. This will result in a simpler superstructure design for fabrication and deployment. Each optimized design also reduces the cross-section depth, thereby reducing the cost and time for transportation. While the GFRP and 483 MPa steel designs were not able to reduce the overall system weight, the 689 MPa steel design does, thereby achieving a design priority of the project.

The results from the authors' study of the re-conceptualized causeway have been presented here. This work is intended as an initial, optimized design upon which a final detailed design would need to be performed. Areas which warrant further study for such a final design include further detailed connection design. Additional finite element analysis could also be performed to determine if it is possible to further reduce the weight by reducing the width of the webs, as the selected width was determined by conservatively assuming that each web would carry the entire shear demand. The cost for material and manufacturing should also be investigated. Finally, the constructability of the proposed cross sections and connection details between components need to be examined. While such future work is necessary to lead to a detailed design, this research has culminated in preliminary, optimized designs for a re-conceptualized, rapidly deployable causeway.

ACKNOWLEDGEMENTS

The authors would like to acknowledge all involved in the design of the Lightweight Modular Causeway System. This research was supported in part by the University of Notre Dame's Center for Research Computing through computational resources.

REFERENCES

AASHTO (2012). *AASHTO Load & Resistance Factor Design (LRFD) Specifications, Customary US Units*. 6th edition American Association of State Highway and Transportation Officials (AASHTO).

Ali, N. B. H., Rhode-Barbarigos, L., Albi, A. A. P., and Smith, I. F. C. (2010). "Design optimization and dynamic analysis of a tensegrity-based footbridge." *Engineering Structures*, 32(11), 3650–9.

Anon. (2012). "Modular causeway systems. Global Security Website. <http://www.globalsecurity.org/military/systems/ship/mcs.htm> (April 21, 2012).

ASCE (2010). *Pre-standard for Load & Resistance Factor Design (LRFD) of Pultruded Fiber Reinforced Polymer (FRP) Structures (Final)*. American Society of Civil Engineers (ASCE) American Composites Manufacturers Associations (ACMA).

Beer, F. P., Johnston, E. R., and DeWolf, J. T. (2006). *Mechanics of Materials*. McGraw Hill Higher Education, Boston, 4th edition.

Buonopane, M. (2002). “Modular Causeway Systems: Hitting the beach with the U.S. Army.” *Proceedings of the Seventh International Conference on Applications of Advanced Technology in Transportation*, ASCE, Cambridge, MA, 241–248.

Deitchman, C. G. (1993). *Possible Logistical Implications of ‘From the Sea’*. Naval War College, Newport, RI (June).

Delta Composites L.L.C. (2004). “Design manual: fiberglass grating and structural products. <http://www.deltacomposites.com/lit_library/DelDesMan.pdf> (January 20, 2013).

Deming, M. A. (2009). “Lightweight Modular Causeway System: Logistics advanced concept technology demonstration.” *Army Logistician*, Professional Bulletin of United States Army Logistics, 50–51.

Department of Defense Office of the Inspector General (2004). *Contract Award and Administration for Modular Causeway Systems (D-2005-021)*. Department of Defense, Arlington, VA (November).

Dey, T. K., Srivastava, I., Khandelwal, R. P., Sharma, U. K., and Chakrabarti, A. (2013). “Optimum design of FRP rib core bridge deck.” *Composites Part B: Engineering*, 45(1), 930–938.

Elbehairy, H., Elbeltagi, E., Hegazy, T., and Soudki, K. (2006). “Comparison of two evolutionary algorithms for optimization of bridge deck repairs.” *Computer-Aided Civil and Infrastructure Engineering*, 21, 561–572.

Federal Republic of Germany, United Kingdom & United States of America (1996). *Trilateral design and test code for military bridging and gap-crossing equipment*. United States.

Ferguson, B. (2010). “State of the art equipment bridges the gap. AMM-TIAC: Advanced Materials, Manufacturing and Testing Information Analysis Center, <http://www.af.mil/news/story.asp?id=123202740> (December 2, 2011).

Fort Eustis Weather (2012). “Pierson - Moskowitz sea spectrum. <http://www.eustis.army.mil/WEATHER/Weather_Products/seastate.htm> (April 26, 2012).

Fowler, J. E., Resio, D. T., Pratt, J. N., Boc, S. J., and Sargent, F. E. (2006). “Innovations for future gap crossing operations.” Engineering Research and Development Center, Vicksburg, MI, 1–5.

Garala, H. J. (2004). “Development of a composite prototype module for the Improved Navy Lighterage System (INLS).” *Proceedings of the Fourteenth International Offshore and Polar Engineering Conference*, International Society of Offshore and Polar Engineers, Toulan, France, 235–243.

Groff, H. L. (1992). “Overview and analysis of the U.S. Navy Elevated Causeway System. MSE Thesis, University of Texas at Austin, Austin, TX.

He, Y. and Aref, A. J. (2003). “An optimization design procedure for fiber reinforced polymer web-core sandwich bridge deck systems.” *Composite Structures*, 60, 183–195.

Kirkpatrick, S., Gelatt, C. D., and Vecchi, M. P. (1983). “Optimization by simulated annealing.” *Science*, 220(4598), 671–680.

Lin, S. S. (1999). “Development of a rapid pile splicer for the Navy Modular Elevated Causway System.” *Proceedings of the Ninth International Offshore and Polar Engineering Conference*, International Society of Offshore and Polar Engineers, Brest, France, 554–557.

Liu, C., Hammad, A., and Itoh, Y. (1997). “Multiobjective optimization of bridge deck rehabilitation using a genetic algorithm.” *Microcomputers in Civil Engineering*, 12, 431–443.

Martí, J. V. and González-Vidosa, F. (2010). “Design of prestressed concrete precast pedestrian bridges by heuristic optimization.” *Advances in Engineering Software*, 41, 916–922.

Martinez-Martin, F. J., Gonzalez-Vidosa, F., Hospitaler, A., and Yepes, V. (2012). “Multi-objective optimization design of bridge piers with hybrid heuristic algorithms.” *Journal of Zhejiang University - Science A*, 13(6), 420–432.

Park, K. T., Kim, S. H., Lee, Y. H., and Hwang, Y. K. (2005). "Pilot test on a developed GFRP bridge deck." *Composite Structures*, 70, 48–59.

Perea, C., Alcala, J., Yepes, V., Gonzalez-Vidosa, F., and Hospitaler, A. (2008). "Design of reinfoced concrete bridge frames by heuristic optimization." *Advances in Engineering Software*, 39, 676–688.

Pham, D. C. and Wang, C. M. (2010). "Optimal layout of gill cells for very large floating structures." *Journal of Structural Engineering*, ASCE, 907–916.

Potts, K. (2009). "Construction during World War II: Managment and financial administration." *Proceedings of the 25th Annual ARCOM Conference*, Association of Researchers in Construction Management, Nottingham, UK, 847–856 (September).

Qu, W., Wang, Y., and Pi, Y. (2011). "Multi-axle moving train loads identification on simply supported bridge by using simulated annealing genetic algorithm." *International Journal of Structural Stability and Dynamics*, 11(1), 57–71.

Resio, D. T., Fowler, J. E., Boc, S. J., Padula, J. A., and Holder, P. M. (2012). "Development and testing of the lightweight modular causeway system. Manuscript in preparation, U.S. Army Engineer Research and Development Center, Vicksburg, MS.

Russell, B. R. and Thrall, A. P. (2013). "Portable and rapidly deployable bridges: Historical perspective and recent technology developments." *Journal of Bridge Engineering*, ASCE.

Skaalen, C. I. and Rausch, A. B. (1977). "Container off-loading and transfer system (COTS) - advanced development tests of elevated causeway system. Volume II - elevated causeway installation and retrieval. Civil Engineering Laboratory, Port Hueneme, CA, 1-22, 31-33.

Suppapitnarm, A., Seffen, K. A., Parks, G. T., and Clarkson, P. J. (2000). "A simulated annealing algorithm for multiobjective optimization." *Engineering Optimization*, 33(1), 59–85.

Thompson, M. D., Eamon, C. D., and Rais-Rohani, M. (2006). "Reliability-based optimization of fiber-reinforced polymer composite bridge deck panels." *Journal of Structural Engineering*, ASCE, 132(12), 1898–1906.

Thrall, A. P. (2011). "Shape-finding of a deployable structure using simulated annealing." *Journal of the International Association for Shell and Spatial Structures*, 52(4), 241–247.

Thrall, A. P., Adriaenssens, S., Paya-Zaforteza, I., and Zoli, T. P. (2012). "Linkage-based movable bridges: Design methodology and three novel forms." *Engineering Structures*, 37, 214–223.

Thrall, A. P., Zhu, M., Guest, J. K., Paya-Zaforteza, I., and Adriaenssens, S. (2013). "Structural optimization of deploying structures comprised of linkages." *Journal of Computing in Civil Engineering*, ASCE Accepted for publication.

Wang, C. M., Pham, D. C., and Ang, K. K. (2007). "Effectiveness and optimal design of gill cells in minimizing differential deflection in circular VLFS." *Engineering Structures*, 29, 1845–1853.

List of Tables

$Type$	$Value$
Moment	1140 kNm
Shear	360 kN
Torison	160 kNm

TABLE 1. Design Moment, Shear, and Torsion. Data courtesy of US Army ERDC [Resio et al 2012]

Parameters						Minimum Area			Minimum Ix		
$Name$	v	pm	r	m	n	μ (m^2) x10^{-1}	σ (m^2) x10^{-3}	c_v	μ (m^4) x10^{-3}	σ (m^4) x10^{-9}	c_v
SA 1	1	10	0.8	5	1	6.22	1.3	0.21	3.50	21	6.1
SA 2	1	10	0.8	10	2	6.22	0.61	0.10	3.50	7.7	2.2
SA 3	1	10	0.9	5	1	6.45	73	11.29	3.50	14	4.1
SA 4	**1**	**10**	**0.9**	**10**	**2**	**6.22**	**0.46**	**0.07**	**3.50**	**7.2**	**2.1**
SA 5	1	10	0.8	5	1	6.23	1.8	0.30	3.50	21	5.9
SA 6	1	10	0.8	10	2	6.36	59	9.35	3.50	13	3.7
SA 7	1	10	0.9	5	1	6.22	1.3	0.20	3.50	35	9.9
SA 8	1	10	0.9	10	2	6.43	94	14.68	3.50	5.4	1.6
SA 9	2	10	0.8	5	1	6.23	1.6	0.26	3.50	33	9.4
SA 10	2	10	0.8	10	2	6.23	1.2	0.20	3.50	42	12
SA 11	2	10	0.9	5	1	6.22	0.68	0.11	3.50	13	3.8
SA 12	2	10	0.9	10	2	6.22	0.96	0.15	3.50	4.5	1.3
SA 13	2	10	0.8	5	1	6.24	1.6	0.26	3.50	40	11
SA 14	2	10	0.8	10	2	6.24	1.3	0.21	3.50	14	3.9
SA 15	2	10	0.9	5	1	6.23	1.1	0.18	3.50	120	34
SA 16	2	10	0.9	10	2	6.22	0.93	0.15	3.50	7.9	2.2

TABLE 2. Simulated Annealing Numerical Tests for GFRP Design. *The first six columns list the name of the combination and the parameters, the next 3 columns provide the results for the minimum weight objective function, and the final 3 columns provide the results for the minimum moment of inertia objective function. The bold row indicates the most robust solution.*

	$LMCS\ Prototype$ $(Aluminum)$	$Design\ 1$ $(GFRP)$	$Design\ 2$ $(483MPa\ Steel)$	$Design\ 3$ $(689MPa\ Steel)$
Modulus of Elasticity (E)	70,000 MPa	12,400 MPa	200,000 MPa	200,000 MPa
Moment of Inertia (I)	0.0016 m^4	0.0035 m^4	0.000217 m^4	0.000220 m^4
EI	112 MN	43.4 MN	43.4 MN	44.0 MN
Density (p)	2,800 kg/m^3	1,790 kg/m^3	7,850 kg/m^3	7,850 kg/m^3
Cross Sectional Area	0.17 m^2	0.63 m^2	0.12 m^2	0.098 m^2
Superstr. Depth (H)	0.319 m	0.222 m	0.111 m	0.118 m
Weight (W) (no hinges, floats)	446 kg/m	1,125 kg/m	942.8 kg/m	766.7 kg/m
Superstr. Weight (no floats)	884 kg/m	1,125 kg/m	942.8 kg/m	766.7 kg/m
System Weight	967 kg/m	1,208 kg/m	1,025.8 kg/m	849.7 kg/m

TABLE 3. Comparison between Original Prototype and Proposed Designs.

List of Figures

FIG. 1. Prototype for rapidly deployable causeway system. Image courtesy of US Army ERDC.

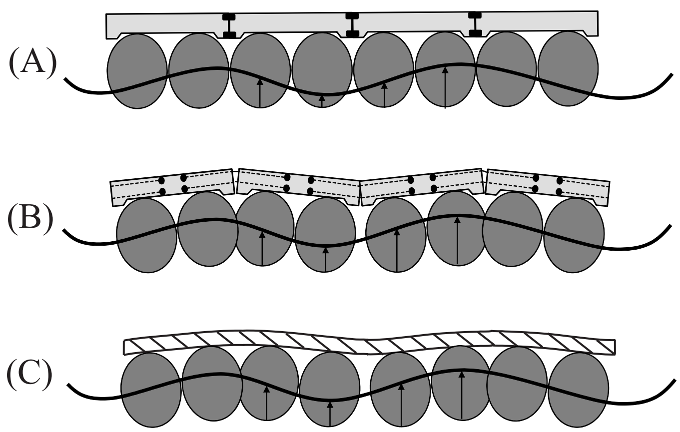

FIG. 2. Three configuration for causeway system: (A) stiff superstructure, (B) hinged superstructure, (C) re-conceptualized superstructure. Images (A) and (B) courtesy of US Army ERDC [Resio et al 2012].

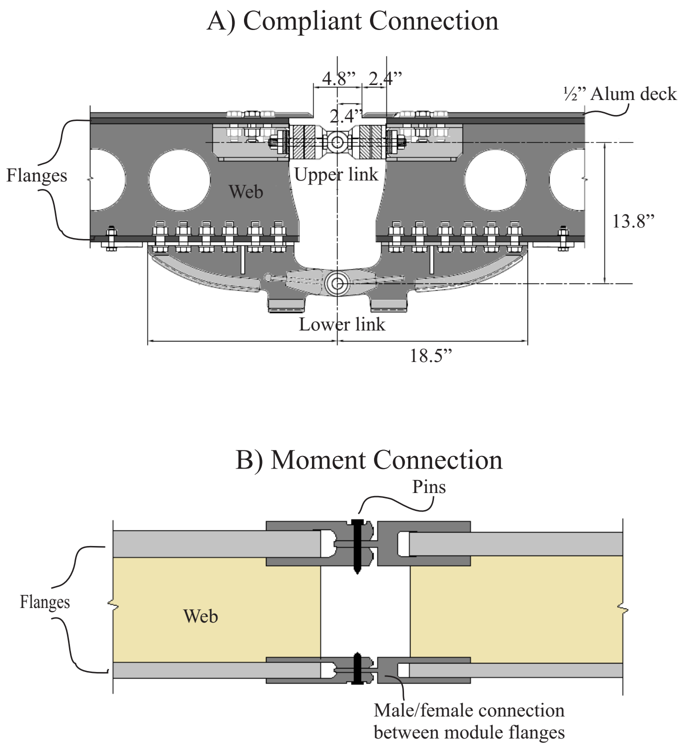

FIG. 3. Hinge configurations: (A) compliant connection in original LMCS design, (B) moment connection for re-conceptualized system. Image (A) based on drawings provided by the ERDC.

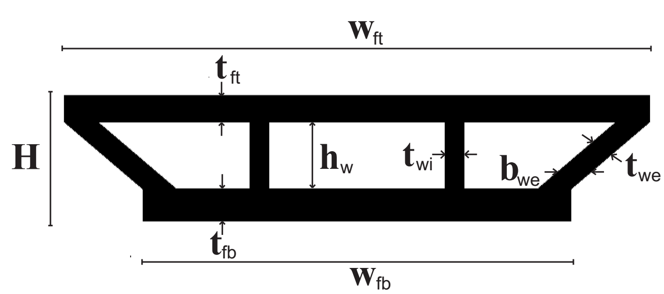

FIG. 4. General Cross Section

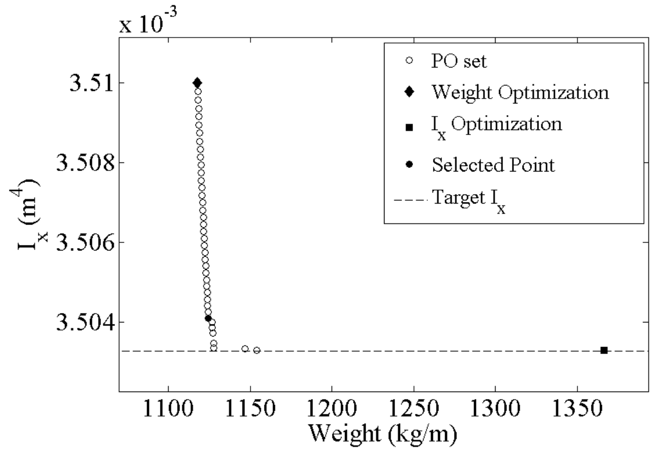

FIG. 5. Pareto-Optimal (PO) Set of Solutions from One MOSA Numerical Simulation

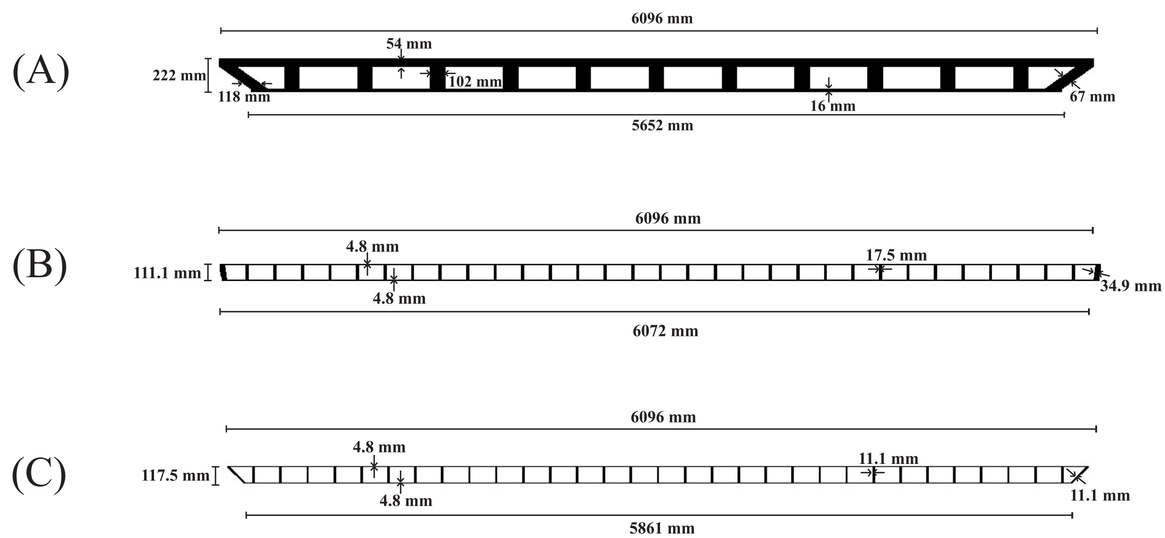

FIG. 6. Optimized Cross Sections in GFRP (A), 483 MPa steel (B) and 689 MPa steel (C)